AIAA JOURNAL
Vol. 42, No. 2, February 2004

Shock-Stall Flutter of a Two-Dimensional Airfoil

Masahide Yamasaki* and Koji Isogai†
Kyushu University, Hukuoka 812-8581, Japan
Takefumi Uchida‡
Toyota Motor Corporation, Toyota 471-8572, Japan
and
Itsuma Yukimura§
Japan Airlines, Tokyo 144-0041, Japan

In an experiment using a single-degree-of-freedom (pitching) flutter model, which simulates the typical section of a forward-swept wing, shock-stall flutter, which is induced by large-scale shock-induced flow separation, has been observed by a schlieren system with a high-speed video camera. The experimental results are compared with computational ones to evaluate the numerical analysis code using the compressible Navier–Stokes equations. The mechanism of the shock-stall flutter is made clear by considering the relations between the pitching moments vs angle of attack and the flow patterns around the airfoil, which are obtained by the experimental flow visualization and the numerical simulation.

Nomenclature

b	=	semichord
C_M	=	pitching-moment coefficient about axis of pitch
f_F	=	flutter frequency
f_N	=	natural frequency
g	=	structural damping of flutter oscillation system
I_α	=	moment of inertia about axis of pitch
k	=	reduced frequency, $b\omega/U$
k_F	=	flutter reduced frequency, $b\omega_F/U$
M	=	freestream Mach number
q	=	dynamic pressure
q_F	=	flutter dynamic pressure
R	=	Reynolds number based on chord
T	=	time
t	=	dimensionless time, $(U/b)T$
U	=	freestream velocity
α	=	angle of attack
α_I	=	initial angle of attack
α_M	=	mean angle of attack
ω	=	circular frequency
ω_F	=	flutter circular frequency

Introduction

IN an experimental study of transonic flutter/divergence characteristics of aeroelastically tailored and nontailored high-aspect-ratio forward-swept wings, an unusual flutter phenomenon was observed for the nontailored wing.[1] The phenomenon has been confirmed qualitatively as shock-stall flutter by a numerical simulation using a two-dimensional (time-averaged) compressible Navier–Stokes equations model.[2]

Received 2 July 2003; accepted for publication 8 October 2003.

*Research Associate, Department of Aeronautics and Astronautics.
†Professor, Department of Aeronautics and Astronautics. Associate Fellow AIAA.
‡Engine Management System Department, Power Train Engineering Division, Power Train Development Center.
§Base Aircraft Maintenance, Haneda Engineering and Maintenance, Aircraft Maintenance Division, Ota-ku.

The shock-stall flutter, which occurs for the nontailored forward-swept wing in transonic range, has the following characteristics, which are different from the conventional (classical type) flutter:

1) The flutter is essentially a single-degree-of-freedom flutter of the first bending mode; the characteristic feature of which is the "wash-in mode" (pivotal point located downstream of the trailing edge) on a typical section (in the flow direction) of a forward-swept wing, as shown in Fig. 1.

2) In the flutter, the large-scale shock–induced flow separation, as shown in Fig. 2, plays a dominant role.

3) The flutter frequency is slightly lower than the first natural frequency of a forward-swept wing.

4) The flutter can occur at unusually low dynamic pressures.

To confirm the results of the numerical simulation, the experimental study is performed by using a single-degree-of-freedom flutter system with a two-dimensional airfoil model, which simulates the typical section of a forward-swept wing. The present study includes flow visualization around the airfoil during the diverging oscillation by a schlieren system with high-speed video camera, in order to confirm the existence and behavior of the large-scale shock-induced flow separation.

Experimental Facility and Technique

The flutter experiments were conducted in the 0.25 m (width) × 0.45 m (height) blowdown transonic wind tunnel of Kyushu University. By numerical simulation[2] using the Navier–Stokes code, it has been shown that the shock-stall flutter is essentially a single-degree-of-freedom flutter of the wash-in mode. Thus the experimental single-degree-of-freedom flutter system (wash-in mode system) with the pivotal point (axis of pitch) located at one chord length downstream from the midchord point, as shown in Fig. 3, was designed. The airfoil section of the model is a natural laminar-flow-type supercritical airfoil with 12% thickness. The airfoil coordinates are given in Table 1. The chord length and the span of the model are 0.1 and 0.252 m, respectively. The airfoil model was made of extra super duralumin and had a wing tip plate at each end of the model to realize two-dimensional flow, as shown in Fig. 4. The plates were made of clear acrylic and coated with silicone to have better schlieren images and attached thin brass-stiffener rings on the both sides of the plates. The arms fixed at both sides of the airfoil are on the outside of the test section of the wind tunnel. The angle of attack of the airfoil was measured by laser displacement sensors, which sensed the displacement of the arms.

The airfoil model was set up at the initial angle of attack of 2 deg. The experiments were performed with three (constant) Mach

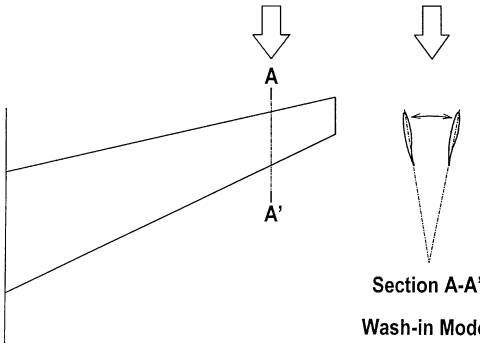

Fig. 1 Characteristics of the first bending mode of (nontailored) forward-swept wing.

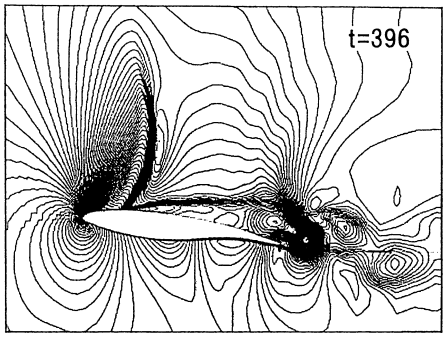

a)

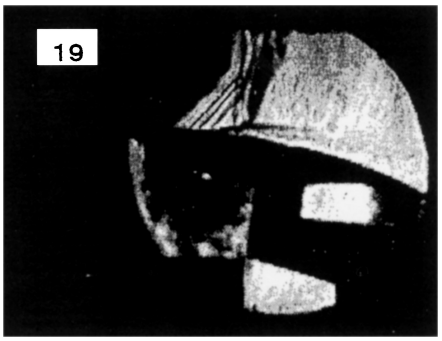

b)

Fig. 2 Large-scale shock-induced flow separation (taken from Fig. 6); a) Isodensity contour obtained by the numerical simulation (E.08): $M = 0.72$ and $k = 0.072$ and b) Schlieren picture: $M = 0.72$ and $k = 0.071$.

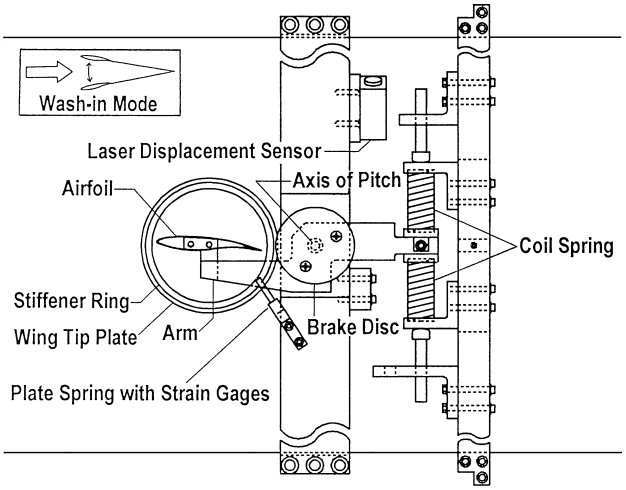

Fig. 3 Experimental single-degree-of-freedom (pitching) flutter system.

Table 1 Natural laminar-flow-type supercritical airfoil

Upper surface		Lower surface	
Station, %	Ordinate, %	Station, %	Ordinate, %
0	0.42	0	0.42
0.19	0.91	0.13	−0.02
0.63	1.42	0.65	−0.49
1.37	2.05	1.47	−0.91
2.43	2.71	2.59	−1.35
3.84	3.33	4.02	−1.83
5.59	3.87	5.77	−2.34
7.68	4.35	7.83	−2.89
10.08	4.78	10.21	−3.45
12.81	5.18	12.92	−4.00
15.87	5.54	15.95	−4.52
19.24	5.86	19.31	−5.00
22.93	6.13	22.99	−5.43
26.95	6.34	26.99	−5.79
31.29	6.49	31.31	−6.06
35.94	6.56	35.96	−6.21
40.92	6.54	40.94	−6.15
46.22	6.42	46.25	−5.80
51.83	6.16	51.89	−5.10
57.78	5.75	57.84	−4.12
64.03	5.15	64.10	−3.06
70.61	4.32	70.66	−2.16
77.50	3.20	77.52	−1.63
84.71	1.70	84.70	−1.62
92.21	−0.24	92.19	−2.24
100.00	−2.41	100.00	−3.08

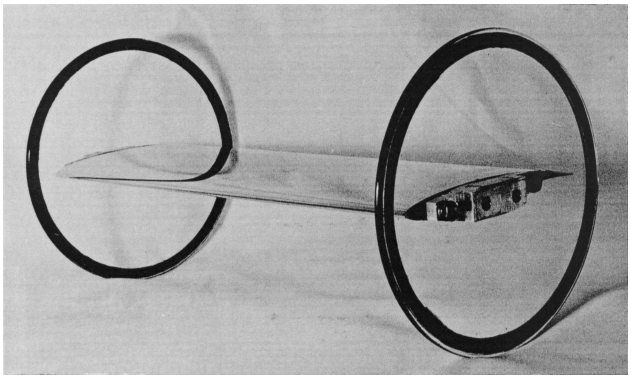

Fig. 4 Experimental airfoil model with wing tip plates.

numbers. During the flutter experiments, the dynamic pressure of the test section has been changed from low to high values to obtain the hard flutter point. A schlieren system with a high-speed video camera was used to observe the flow around the airfoil during the diverging oscillation. A He–Ne laser of 5 mW was used as the light source of the system. To make noiseless point source, a special filter was used. The knife edge was set almost perpendicularly to the flow direction. The schlieren images were taken by the video camera at a frame speed of 2000 frames/s and a shutter speed of 1/20,000 s.

Results and Discussion

The natural vibration characteristics and the experimental conditions and results are shown in Table 2, which includes the results of the numerical analysis (E.08) that has been performed with the same experimental condition as the one of the experiment (E.08), except for the initial angle of attack. The aeroelastic response computation has been performed by using a two-dimensional (time-averaged) compressible Navier–Stokes code,[2,3] which employs the Yee–Harten total-variation-diminishing (TVD) scheme[4] and the Baldwin and Lomax turbulence model.[5] The number of grid points employed is 280×80 with 200 points on the airfoil. The present computation has been performed at the initial angle of attack $\alpha_I = 0$ deg, whereas the initial angle of attack in the experiment is $\alpha_I = 2$ deg. This is because the computation at $\alpha_I = 2$ deg diverged.

Table 2 Vibration and flutter characteristics

Property	Experiment (E.08)	Numerical analysis (E.08)	Experiment (E.09)	Experiment (E.10)
Natural frequency f_N, Hz	61.4	61.4	61.4	61.4
Structural damping g	0.025	0.025	0.025	0.025
Moment of inertia about axis of pitch I_α, kg-m^2	15.7×10^{-3}	15.7×10^{-3}	15.7×10^{-3}	15.7×10^{-3}
Initial angle of attack α_I, deg	2	0	2	2
Reynolds number based on chord R	1.13×10^6	1.13×10^6	1.44×10^6	1.49×10^6
Flutter frequency f_F, Hz	54.7	57.6	53.9	52.9
Flutter reduced frequency k_F	0.071	0.074	0.074	0.075
Freestream Mach number M	0.72	0.72	0.68	0.65
Flutter dynamic pressure q_F, kPa	49	42	58	58
Mean angle of attack α_M, deg	7.6	3.2	8.6	8.8

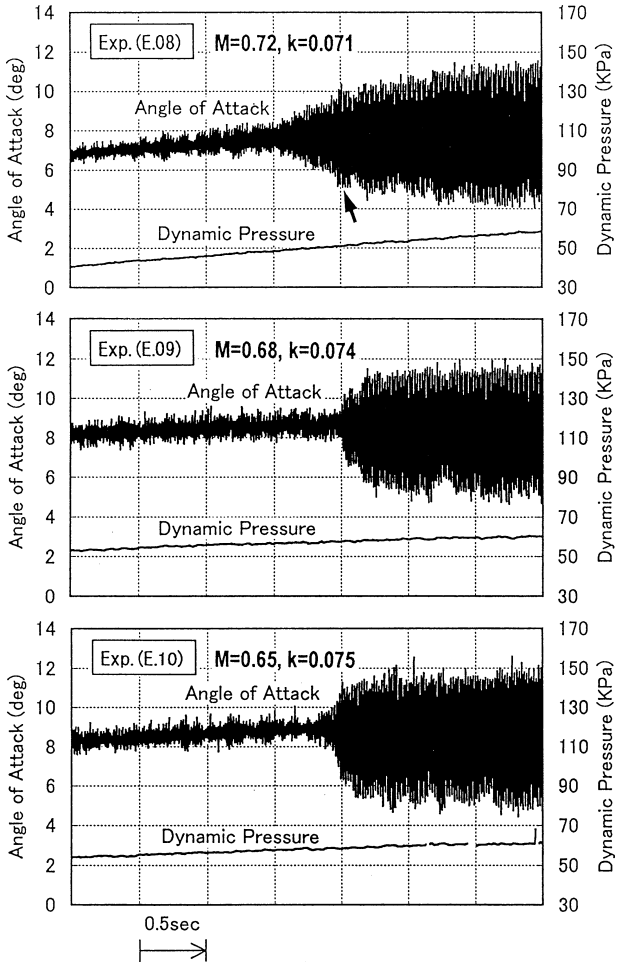

Fig. 5 Responses of angle of attack with increasing dynamic pressure.

The flutter frequencies in the experiments are lower than the natural frequency, in the same way as the flutter frequency in the numerical analysis. This is one of the things characterizing shock-stall flutter. In Table 2, the flutter reduced frequency k_F in the numerical analysis is slightly higher than the one in the experiment. The flutter dynamic pressure q_F in the numerical analysis is lower than the one in the experiment. The mean angle of attack α_M in the numerical analysis is lower than one-half of the experiment. As just mentioned, some discrepancies on the flutter characteristics are seen between the results of the experiments and the numerical analysis.

The responses of the instantaneous angle of attack with the increasing dynamic pressure, obtained at three Mach numbers, are shown in Fig. 5. In the case of Exp. (E.08) at Mach number $M = 0.72$, the flutter is more soft, and the flutter dynamic pressure is lower than with other ones.

As an example of the schlieren-pictures series taken by the high-speed video camera during the flutter oscillation, the series of about one cycle pointed by an arrow in experiment (E.08) of Fig. 5, is compared, in phase, with the flow patterns (isodensity contour) obtained by the numerical simulation, which corresponds with the experiment (E.08) except for the initial angle of attack, in Figs. 6a and 6b, where the arrows show the direction of time flow. Picture numbers 0, 18, and 37 almost coincide with the ones of the minimum, maximum, and minimum angles of attack, respectively. One cycle of the flutter oscillation corresponds to 36.6 frames of the picture series. The large-scale shock-induced flow separations characterizing the shock-stall flutter are observed clearly.

On both results of the experiments and the numerical simulations, the shock wave that has appeared on the upper surface of the airfoil becomes clear with the increasing angle of attack. Then the separations from the root of the shock wave occurs at the phase between the pictures 14 and 15. The separations, shown by the numerical simulation, occur at about the same phase between the dimensionless times $t = 378$ and 384 as the experimental one. The appearance of the separation causes a change in the pitching-moment coefficient C_M from increasing to decreasing, shown in Fig. 7, where the direction of the change in C_M is shown by the arrows. Then the shock waves move to the leading edge of the airfoil with the increasing angle of attack for both the results of the experiments and the numerical simulation. The movement of the shock wave causes the increase of the separated area. C_M, from $t = 384$ to 402, decreases abruptly with the increasing separated area. In the experiments, the large-scale separation disappears about at the same phase (picture number 27) as the one between $t = 408$ and 414 in the numerical simulation. It seems that the disappearance of the separation causes the recovering of C_M in Fig. 7. The flutter is caused by the hysteresis loop of C_M vs the angle of attack α. When the area surrounded by the anticlockwise loop is subtracted from the one surrounded by the clockwise loop, the remainder corresponds with the work done on the airfoil motion by the pitching moment. If the remainder becomes positive, the flutter occurs. As a typical example of the relations between the hysteresis and the flow patterns around the airfoil, it can be presented that the isodensity contours around the airfoil at $t = 384$ and 408, when the angles of attack are almost the same, are quite different. This is similar to the experiments. That is to say, at each time, the sizes of the separated area, which are determined by the positions of the shock wave, are quite different. It can be considered that their area sizes cause a large difference of C_M.

On the whole, the flow patterns obtained by the numerical simulation are almost the same as those obtained by the experimental flow visualization. As shown in Table 2, there are discrepancies between the flutter characteristics in the experiments and those in the numerical analysis. One of the reasons for these discrepancies can be attributed to the computation at the initial angle of attack $\alpha_I = 0$ deg, which is different from $\alpha_I = 2$ deg in the experiment. Another reason can be attributed to the inadequacy of the Baldwin and Lomax turbulence model employed in the numerical simulation for treating the large-scale shock-induced flow separation.

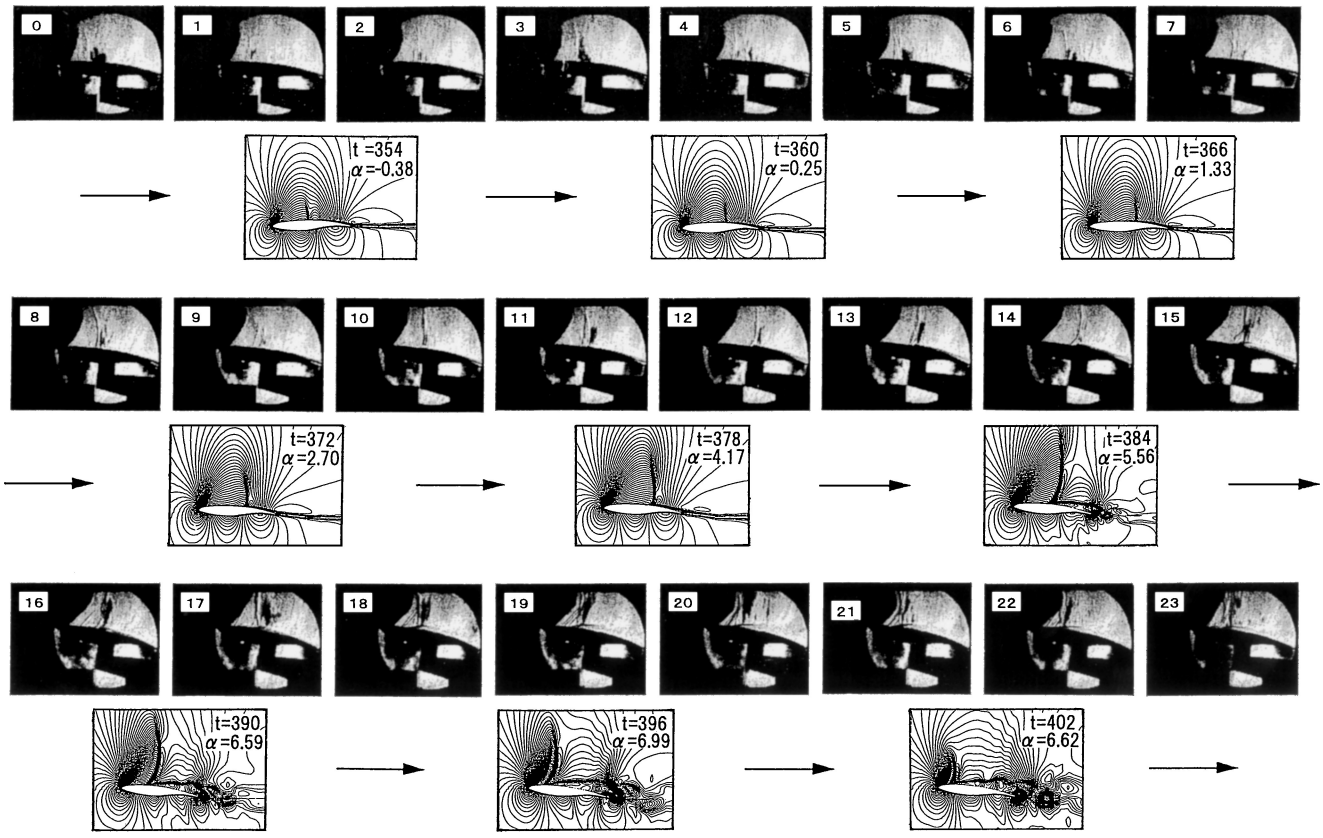

Fig. 6a Comparison, in phase, of experimental and computed flow patterns (E.08) with $M = 0.72$ and $R = 1.13 \times 10^6$: first row, schlieren pictures ($k = 0.071$, $\alpha_I = 2$ deg, and $q = 51$ kPa, and second row, isodensity contour obtained by the numerical simulation ($k = 0.072$, $\alpha_I = 0$ deg, and $q = 49$ kPa).

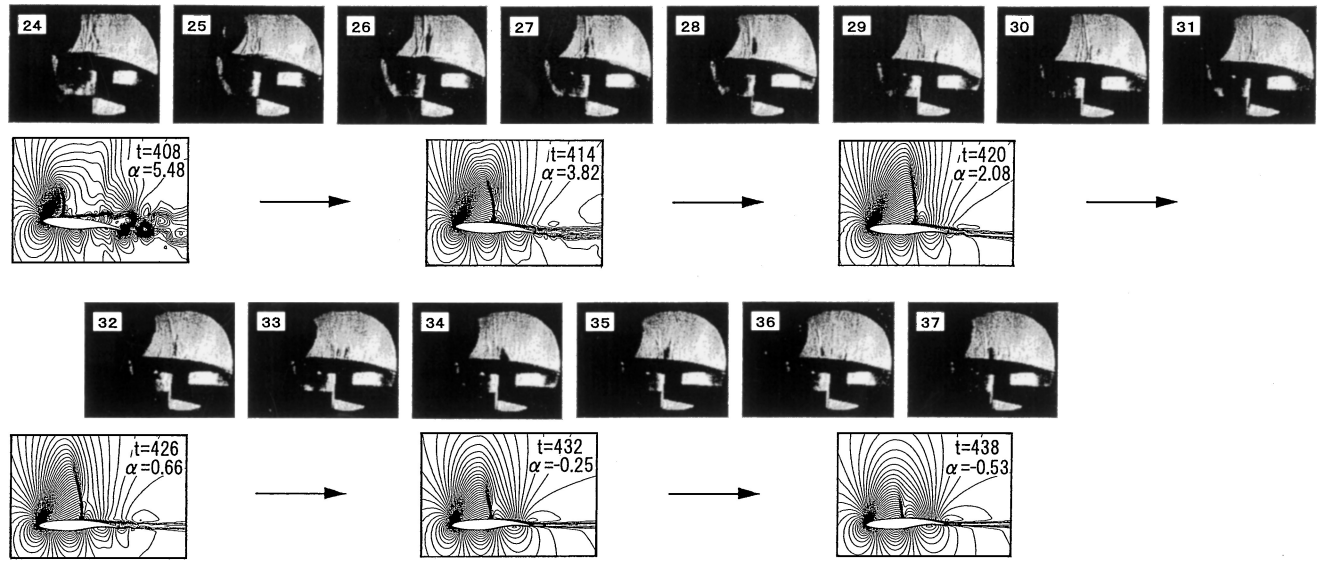

t : dimensionless time, (U/b)T
U : free stream velocity
b : semi-chord
T : time
α: angle of attack (deg.)

Fig. 6b Continued from Fig. 6a for still larger *t*.

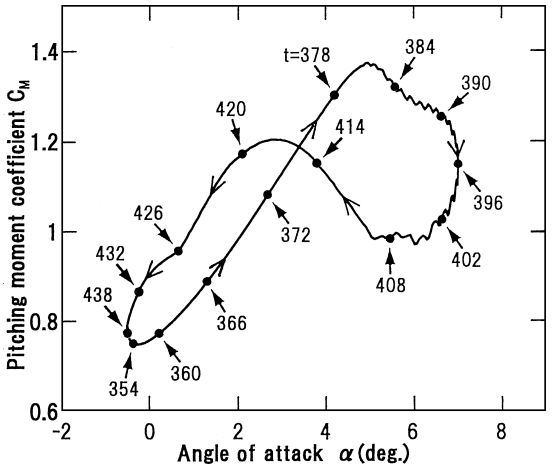

Fig. 7 Behavior of pitching moment about pivotal point on $C_M \sim \alpha$ plane: $M = 0.72$, $R = 1.13 \times 10^6$, $k = 0.072$, $\alpha_I = 0$ deg, and $q = 49$ kPa.

Conclusions

Shock-stall flutter, with some characteristics, which had been predicted by the numerical simulation using the Navier–Stokes code, was observed in the present experiments that were performed using a single-degree-of-freedom flutter system, which simulated a typical section of a forward-swept wing. By flow visualization and numerical simulation, it was confirmed that the shock-stall flutter was caused by the hysteresis of the pitching-moment coefficient vs angle of attack and the hysteresis was caused by the change of the large-scale shock–induced flow separation area during the flutter oscillation of the airfoil.

Although there were discrepancies on the flutter characteristics between the results of the experiments and the ones of the numerical analysis, it is believed that the experimental data at the transonic region obtained in this study can be used as the experimental benchmark test data for evaluating two-dimensional Navier–Stokes codes with various turbulence models.

References

[1]Isogai, K., "Transonic Flutter/Divergence Characteristics of Aeroelastically Tailored and Non-Tailored High-Aspect-Ratio Forward-Swept Wings," *Journal of Fluids and Structures*, Vol. 6, 1992, pp. 525–537.

[2]Isogai, K., "Numerical Simulation of Shock-Stall Flutter of an Airfoil Using the Navier–Stokes Equations," *Journal of Fluids and Structures*, Vol. 7, 1993, pp. 595–609.

[3]Isogai, K., Shinmoto, Y., and Watanabe, Y., "Effects of Dynamic Stall on Propulsive Efficiency and Thrust of Flapping Airfoil," *AIAA Journal*, Vol. 37, No. 10, 1999, pp. 1145–1151.

[4]Yee, H. C., and Harten, A., "Implicit TVD Schemes for Hyperbolic Conservation Laws in Curvilinear Coordinates," *AIAA Journal*, Vol. 25, No. 2, 1987, pp. 266–274.

[5]Baldwin, B. S., and Lomax, H., "Thin Layer Approximation and Algebraic Model for Separated Turbulent Flows," AIAA Paper 78-257, Jan. 1978.

E. Livne
Associate Editor